Broadened Far-Infrared Absorption Spectra for Hydrated and Dehydrated Myoglobin

Chenfeng Zhang,† Enver Tarhan,† A. K. Ramdas,† A. M. Weiner,‡ and Stephen M. Durbin*,†

Department of Physics and School of Electrical and Computer Engineering, Purdue University, West Lafayette, Indiana 47907

Received: January 6, 2004; In Final Form: March 18, 2004

The far-infrared absorption spectra of myoglobin powder at hydration levels between 3.6 and 42 wt % were measured with terahertz time-domain spectroscopy and Fourier transform infrared spectroscopy. Absorption is dominated by the water content, but even the driest specimens have a nearly continuous spectrum without identifiable sharp features. Inhomogeneous broadening plus the intrinsically high spectral density of vibrational modes in the region below 2.0 THz apparently combine to obscure the lowest frequency vibrational modes expected for protein molecules of this size. A continuous absorption spectrum for hydrated protein powders suggests that the absorption mechanisms are similar to those in liquid water, and hinders the spectroscopic identification of biomolecules in this frequency range.

I. Introduction

Terahertz time-domain spectroscopy (THz-TDS)[1−3] bridges the gap between microwaves and far-infrared (far-IR) and has proven to be a promising technique in numerous applications.[4] THz-TDS compares favorably to Fourier transform infrared (FTIR) spectroscopy[5] due to its high brightness, stable, single-cycle pulse generation, and coherent, time-gated detection that greatly reduces the thermal background. These features make it suitable for THz studies of dielectrics and semiconductors,[6] thin films,[7,8] liquids,[9−11] gases,[12−14] and superconductors.[15,16]

Furthermore, there are now numerous THz studies of large biomolecules such as DNA,[17−19] proteins,[17,20] and other biological molecules.[21,22] Infrared and far-infrared vibrational dynamics of macromolecules are of significant interest for understanding the functional mechanisms in large biomolecules.[23,24] The binding of small molecules at the active sites of certain proteins, for example, may be coupled to specific normal modes that include collective motions of the protein at THz frequencies and are important to protein function.[25,26]

While THz radiation should be particularly useful for detecting the low-frequency modes of large molecules, the properties of the small polar molecule H_2O (water) provide a useful starting point for understanding the basic features of THz absorption. THz-TDS results for water vapor show a characteristic set of sharp peaks that serve as a "fingerprint" for this species of isolated molecules (or perhaps small clusters of molecules).[12,27,28] These spectra are easily obtained just from the humidity content in standard laboratory air, because the large electric dipole moment of the water molecule allows for strong coupling to THz radiation. On the other hand, the absorption spectrum of liquid water is a smooth continuum without sharp peaks.[9,29,30] Models generally assume that some combination of collective translational and rotational motions is responsible for this dramatic change from sharp absorption lines in isolated molecules to the continuous absorption in the liquid state.[31]

We report here on THz-TDS investigations of myoglobin (Mb) powder at several hydration levels between 3.6 and 42 wt %. Mb is a relatively simple and well-studied protein, for which the calculated vibrational normal mode density shows a relatively smooth curve with a few distinct peaks in the THz region.[32−34] The role of water in Mb will be of critical importance, since the biological functioning of proteins requires water, and the presence of any water in a protein specimen is likely to have a strong effect on the THz absorption spectrum. Although only powder specimens were studied, including one that was essentially dehydrated, measurements all showed structureless spectra, as with liquid water, and no characteristic sharp lines of the type seen in water vapor and predicted by Mb calculations. That Mb molecules in a fixed, dry state have no distinct peaks raises questions about the role of conformational disorder, inhomogeneous broadening, and other possible mechanisms. These observations have implications on the interaction of protein with the incorporated "biological water", and on the difficulty in identifying biological macromolecules through their THz absorption structures.

II. Experimental Methods

Described below are the procedures used to prepare Mb powders with well-defined hydration levels and the experimental setup for THz-TDS measurements.

II.1. Sample Preparations. The horse heart Mb lyophilized powder was purchased from Sigma and used without further purification. The samples at various hydration levels were obtained by allowing as-received lyophilized powder to equilibrate with different saturated salt solutions in desiccators over several days. The various saturated salt solutions have different measured equilibrium relative humidities (ERH), as indicated in Table 1.[35]

Two samples were prepared side by side for each hydration level. The water content of one was determined by placing it in a sand bath (a beaker with a layer of sand at the bottom) and heating to just above 100 °C for 1 h. All water in the sample is assumed to be removed in this process. The sample was weighed before and after heating; the weight loss was assigned to the

* Author to whom correspondence should be addressed. Phone: 001-765-4946426. Fax: 001-765-4940706. E-mail: durbin@physics.purdue.edu.
† Department of Physics.
‡ School of Electrical and Computer Engineering.

10.1021/jp049933y CCC: $27.50
Published on Web 06/08/2004

TABLE 1: Hydration Results for Mb Powders[a]

soln used for sample prep	equilibrium rel humidity (ERH), %	total sample mass, mg	water content, wt %
KNO_3	86	13.9	42.4
KCl	80	11.8	32.2
NaCl	73	10.5	19.0
NaOH	18	8.4	3.6

[a] Specimens were stored for 3−4 days in a sealed desiccator with one of several saturated salt solutions (column 1) that have specific measured equilibrium relative humidities (column 2). The final weight of the samples and the water content deduced by weight loss upon heating to 100 °C are listed in columns 3 and 4.

original water content of the specimen. The measurement procedure was performed in room air with relative humidity around 40%. Data were recorded as quickly as possible (within 30 s) to exclude any interference from ambient water vapor.

The sample cell is made of two 3.18 mm thick pieces of high-density polyethylene (HDPE) clamped together, with a surface recess in the center of one piece to hold the Mb powder. The cylindrical recess has a diameter of 12.7 mm and a depth of either 1.00 or 0.50 mm (for higher water content samples with strong absorption). While preparing the sample, care was taken to ensure that the recess was uniformly filled with the various Mb powders. Because THz radiation corresponds to wavelengths of $\sim$300 μm, which is much larger than typical Mb particle sizes, elastic scattering effects from the particle are expected to be negligible. HDPE was used because it is almost transparent in the THz range. Vacuum grease was applied between the two HDPE pieces as a sealant to maintain the hydration level of the enclosed sample.

We found that the as-received lyophilized Mb powder has a typical water content of 10 wt %. When the equilibrium relative humidity of the saturated salt solutions is very low, e.g. 18% for the NaOH solution, the equilibrated samples have water content even lower than 10 wt %. This is to say, lyophilized samples could be further dehydrated by this process.

II.2. Experimental Setup. The THz-TDS system used here was purchased from Picometrix, Inc.; details and operating procedures are described elsewhere.[36,37] The experimental setup is illustrated in Figure 1. The light source used is a femtosecond (fs) mode-locked Ti:sapphire laser (100 fs pulse width, 800 nm central wavelength). The THz transmitter (Tx) is a dc-biased photoconductive antenna fabricated on a GaAs substrate, which emits THz radiation in free space. Appropriate lenses are used to manipulate the THz pulse in free space. The focused spot size of the THz beam at the sample location, which is the diameter where the beam intensity drops to 1/e of its peak value, is less than 5 mm. Since the surface recess for holding the sample has a diameter of 12.7 mm, as discussed in Section II.1, no additional aperture is applied to narrow the beam down. On the detector side, the photoconductive antenna (receiver, Rx) with a delayed fs laser probe is driven by the transmitted THz pulse. The signal recorded eventually is the transmitted time-dependent THz electric field. This time-domain waveform is then processed by fast Fourier transform (FFT) to obtain the frequency domain spectrum. The scan time window is about 70 ps, resulting in a spectral resolution of around 0.5 cm^{-1} (15 GHz). The scan rate of the delay stage is 5 ps/s, so it takes about 14 s to run a single scan. To increase the signal-to-noise ratio (SNR), 16 scans were recorded and averaged by the computer to obtain one measurement, corresponding to a data collection time of about 4 min. The resulting SNR is above 3000:1. To further account for system stability issues, multiple measurements were taken for one sample and the data were averaged to obtain the final spectrum (Section 4). All measurements were taken at room temperature.

Because single mode fibers are used to deliver the fs pulse to the transmitter and receiver in the THz spectrometer, there will be positive group velocity dispersion (GVD) imparted onto the pulse as it travels along the fiber. To compensate for this dispersion, a grating-dispersion compensator (GDC) is applied before the laser pulse is coupled into the fiber, which imparts a compensating negative GVD onto the pulse. An optical isolator prevents back-reflections from perturbing the stability of the Ti:sapphire laser. For real time diagnostics of the laser performance, small fractions of the laser power are split off to a spectrometer and an autocorrelator to monitor the spectrum and pulse width of the laser, respectively. Nitrogen gas boil-off from a liquid nitrogen tank is used to purge the THz spectroscopy system to eliminate absorption from ambient water vapor.

III. Material Parameters Extraction Procedure

Data analysis procedures for determining the intrinsic optical properties of the Mb powders from the THz-TDS data are described below.

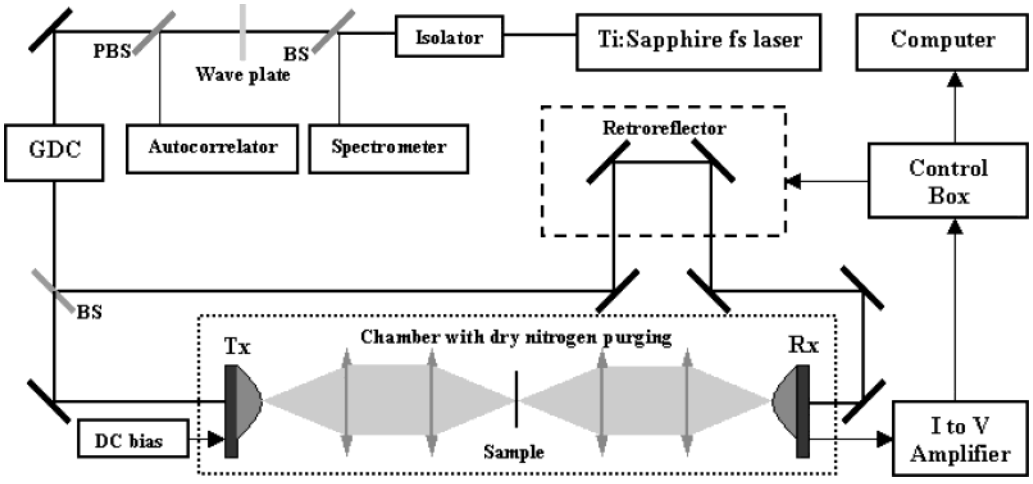

Figure 1. Experiment layout. THz optics are within the dashed box, showing the transmitter (Tx), receiver (Rx), and lenses for collecting the radiation and focusing onto the sample, all within a chamber that can be purged with dry nitrogen gas to remove water absorption effects. External components show the femtosecond laser with a magnetooptic isolator, beam splitter (BS), polarization beam splitter (PBS), and spectrometer and autocorrelator for monitoring beam pulse quality. The grating dispersion compensator (GDC), time-delay retroreflector, and various controls and a computer manage the measurement and data collection process.

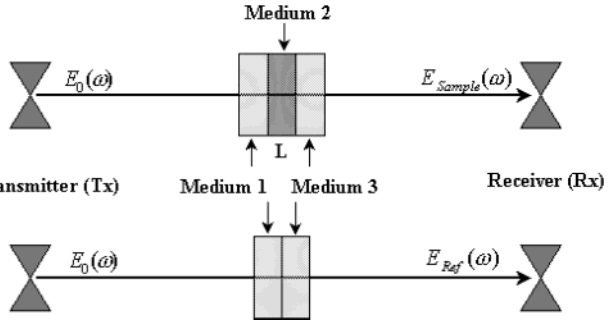

Figure 2. Measurement scheme, requiring one measurement without a sample, and another with a sample (Medium 2) of length L. The sample holder (Mediums 1 and 3) is constructed of high-density polyethylene (HDPE).

III.1. Refractive Index of HDPE. Because HDPE is nearly transparent in the frequency range of interest (0.2−2 THz), the imaginary part of its refractive index is nearly zero (as confirmed by our measurements). We further assume that there is negligible pulse distortion due to GVD of the THz pulse in HDPE, so the only effect on the pulse while it transmits through an HDPE plate is a time delay that depends on the refractive index of the material and its thickness.

The refractive index of the HDPE can be written as

$$n_{\mathrm{HDPE}} = n_{\mathrm{Air}} + \frac{c\Delta t}{l} \tag{1}$$

where n_{Air} is the refractive index of air, c is the speed of light in a vacuum, Δt is the time delay, and l is the thickness of the HDPE plate. For an HDPE plate 3.059 mm thick, we obtained a refractive index of $n_{\mathrm{HDPE}} = 1.533 \pm 0.007$, which is consistent with the accepted value of around 1.5.[38] Further data analysis confirms that the refractive index of HDPE is essentially frequency-independent, with a variation of less than 0.01 over the usable frequency range (0.2−2.0 THz).

III.2. Algorithm for Material Parameters Extraction. One important problem in THz-TDS is how to extract the material parameters reliably from the time-domain waveforms.[39] A commonly used method is to record the waveform twice, in the presence and absence of the sample to be characterized. As shown in Figure 2, Mediums 1 and 3 are the HDPE sample cell plates, and Medium 2 is the Mb specimen. For the reference measurement, instead of leaving an air gap between two pieces of HDPE with a surface recess, we clamped two identical HDPE plates together so that the Fabry−Perot factor from an air gap need not be considered (see eq 2b). The recorded profiles show the temporal dependence of the THz electric field amplitude. Their Fourier transforms, $E_{\mathrm{Sample}}(\omega)$ and $E_{\mathrm{Ref}}(\omega)$, give the spectral components at angular frequency ω of the THz electric field in the presence and absence of the sample:

$$E_{\mathrm{Sample}}(\omega) = \eta(\omega)\, E_0(\omega)\, T_{12}(\omega)\, P_2(\omega,L)\, \mathrm{FP}(\omega)\, T_{23}(\omega) \tag{2a}$$

$$E_{\mathrm{Ref}}(\omega) = \eta(\omega)\, E_0(\omega)\, T_{13}(\omega)\, P_{\mathrm{Air}}(\omega,L) \tag{2b}$$

$\mathrm{FP}(\omega)$ is the factor accounting for the Fabry−Perot effect in the sample:

$$\mathrm{FP}(\omega) = \sum_{k=0}^{+\infty} \{R_{23}(\omega)\, P_2^{\,2}(\omega)\, R_{21}(\omega)\}^k \tag{3}$$

In these equations, $R_{ab}(\omega) = (\tilde{n}_a - \tilde{n}_b)/(\tilde{n}_a + \tilde{n}_b)$ is the reflection coefficient at the $a-b$ interface and $T_{ab}(\omega) = 2\tilde{n}_a/(\tilde{n}_a + \tilde{n}_b)$ is the transmission coefficient from medium a to medium b. $P_a(\omega,L) = \exp(-i\tilde{n}_a\omega L/c)$ is the propagation coefficient in medium a over a distance L. $\tilde{n}_a = n_a - i\kappa_a$ is the complex refractive index of medium a. All the reflection, transmission, and propagation coefficients in the sample cell (Mediums 1 and 3) are included in $\eta(\omega)$. In eq 3, the sum takes into account all reflections within the sample (Medium 2). However, only the first, which occurs at a delay of about 8 ps after the main peak, needs to be considered, because higher order reflections have amplitudes below the noise level and are not detectable. The first echo corresponding to multiple reflections within an individual HDPE sample cell wall occurs at a delay of 20 ps, which is outside the time range of interest. In the actual experiment, a cutoff time at about 17 ps after the main peak was applied and the THz signal later than 17 ps was set to zero to filter out the echoes due to the HDPE sample cell wall.

The complex transmission coefficient of the sample is obtained by dividing $E_{\mathrm{Sample}}(\omega)$ by $E_{\mathrm{Ref}}(\omega)$ (let Mediums 1 and 3 be HDPE and Medium 2 be Mb so $T_{13}(\omega)$ in eq 2b is unity):

$$T(\omega) = \frac{4n_{\mathrm{HDPE}}\tilde{n}_{\mathrm{Mb}}}{(n_{\mathrm{HDPE}} + \tilde{n}_{\mathrm{Mb}})^2} \exp(-i\omega(\tilde{n}_{\mathrm{Mb}} - n_{\mathrm{Air}})L/c)\, \mathrm{FP}(\omega) \tag{4a}$$

with

$$\mathrm{FP}(\omega) = \frac{1}{1 - \left(\dfrac{\tilde{n}_{\mathrm{Mb}} - n_{\mathrm{HDPE}}}{\tilde{n}_{\mathrm{Mb}} + n_{\mathrm{HDPE}}}\right)^2 \exp(-2i\tilde{n}_{\mathrm{Mb}}\omega L/c)} \tag{4b}$$

What we must solve is an inverse electromagnetic problem, i.e., extracting the complex refractive index of the sample $\tilde{n}_{\mathrm{Mb}} = n_{\mathrm{Mb}} - i\kappa_{\mathrm{Mb}}$ from the measured transmission coefficient. Fabry−Perot effects due to surface reflections can produce artificial oscillations on the absorption spectrum, and tend to complicate the interpretation of the experimental results.[17,40]

For this analysis, we employed the algorithm presented by Duvillaret et al.[39] An error function with n_{Mb} and κ_{Mb} as variables characterizing the difference between the theoretical and experimental transmission coefficient is defined, and an iterative procedure performed to obtain refined material parameters until the error is lower than a preassigned value related to the experimental uncertainty. In this algorithm, the Fabry−Perot factor is treated as a perturbation and taken into account in each loop. This extraction procedure for the frequency-dependent complex refractive index function assumes a measured sample thickness L. The precision of the sample thickness measurement proved to be critical for the accuracy of the extracted parameters.[41] A modification to the algorithm allowed us to determine the thickness and the complex refractive index of the sample simultaneously.[42] In this method, the complex refractive index of the sample was determined applying the above algorithm at each trial thickness over a range around the measured sample thickness. Once the material parameters $\tilde{n}_{\mathrm{Mb}} = n_{\mathrm{Mb}} - i\kappa_{\mathrm{Mb}}$ were obtained for a particular thickness l, a total variation metric was defined as follows to measure the smoothness of the complex refractive index function with frequency at this thickness

$$D(\omega_m) = |n_{\mathrm{Mb}}(\omega_m) - n_{\mathrm{Mb}}(\omega_{m-1})| + |\kappa_{\mathrm{Mb}}(\omega_m) - \kappa_{\mathrm{Mb}}(\omega_{m-1})| \tag{5a}$$

$$\mathrm{TV} = \sum_m D(\omega_m) \tag{5b}$$

where the index m denotes frequency. The total variation (TV)

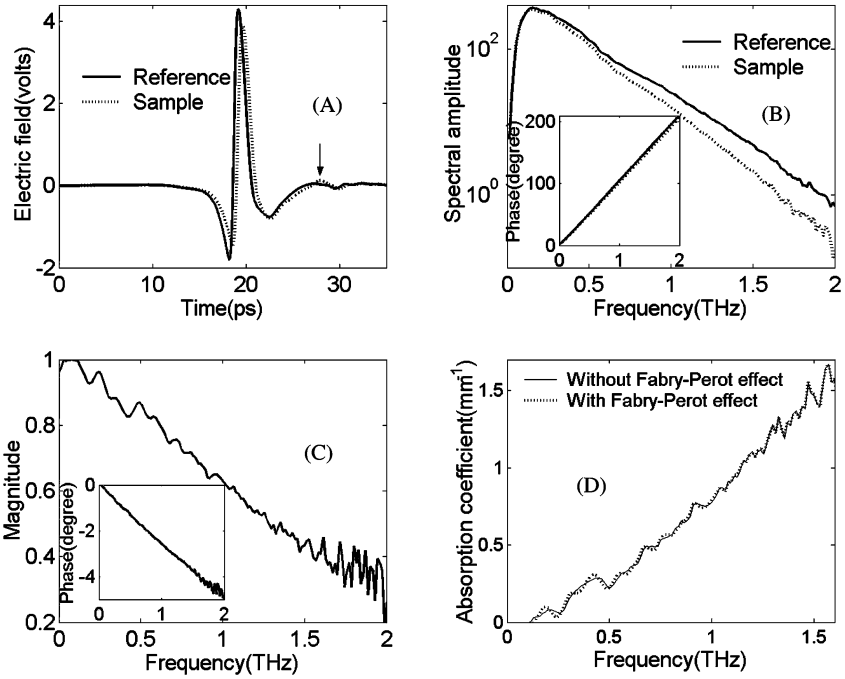

Figure 3. Data collection and analysis for Mb powder at 19.0 wt % water content. (A) Comparison of time spectra recorded without sample (solid line) and with Mb powder (dotted) in the N_2-purged chamber; the arrow denotes the first Fabry−Perot reflection within the sample cell. (B) Fourier transform frequency spectra of the two signals, plus their phase angle (inset). (C) Ratio of amplitudes versus frequency,and phase difference (inset). (D) Calculated absorption coefficient (mm^{-1}) before (dotted line) and after (solid line) correcting for Fabry−Perot oscillations due to sample cell dimensions.

is a function of thickness and its value measures the ruggedness of the retrieved complex refractive index curve. The fewer oscillations the retrieved complex refractive index curve has, the smaller the total variation metric will be. The sample thickness L_0 was identified by the deepest local minimum of TV[42] and the sample parameters can then be calculated at L_0.

Figure 3 gives an example of this absorption spectrum determination procedure. The echo due to reflections from the front and back interfaces of the sample with the sample cell can be seen about 8 ps after the main peak in the time domain waveform (see arrow in Figure 3A). This echo is responsible for the Fabry−Perot oscillations seen below 1.0 THz in the transmission amplitude spectrum (Figure 3C). The phase information is shown as an inset in both the FFT frequency domain spectrum (Figure 3B) and the complex transmission spectrum (Figure 3C). The complex refractive index of the sample can be extracted from the complex transmission spectrum, and the absorption spectrum of the sample can be calculated thereafter. In Figure 3D, the comparison between the absorption spectrum with and without Fabry−Perot effect illustrates a reduction of Fabry−Perot oscillations. The oscillations at low frequencies caused by the sample thickness are reduced when the Fabry−Perot factor is included as a perturbation in the extraction algorithm.

The plots in Figure 3 illustrate the two main sources of uncertainty in the interpretation of THz-TDS data. The first is the Fabry−Perot effect just mentioned, where the sample thickness itself is the source of peaks in the low-frequency region of the deduced absorption spectrum. Any determination of a peak in a THz-TDS absorption spectrum should include a demonstration that the presumed spectral feature is in fact independent of the specimen configuration. The second problem is large noise peaks seen at higher frequencies, caused by the baseline noise from the spectrometer. That is, the output signal consists of the real signal plus a background level that is nearly independent of frequency. If the specimen is strongly absorbing, the high-frequency amplitudes typically are more strongly affected, and the output signal above a given frequency may be entirely due to background noise. The peaks seen above 1.5 THz in Figure 3C,D are largely due to this background effect. Thinner, less absorbing specimens are required to obtain better data at these frequencies.

IV. Results and Discussions

Experimental results are presented and discussed below. Applying the algorithm described previously, we calculate the complex refractive index function of the samples under study based on the measured time-domain waveforms. To validate the THz-TDS measurements, absorption spectra were also measured with FTIR spectroscopy. Comparison between these two measurements yields good agreement.

IV.1. Absorption Spectrum of Mb with a Quadratic Fit. What we have discussed so far is extracting the complex refractive index of the sample from the THz-TDS data. Of particular interest is its absorption spectrum, i.e., the frequency-dependent absorption coefficient. This is related to the imaginary part of the complex refractive index:

$$\alpha_{\mathrm{Mb}} = \frac{4\pi\kappa_{\mathrm{Mb}}}{\lambda} \tag{6}$$

where κ_{Mb} is the imaginary part of the complex refractive index and λ is the wavelength. The sample densities were used to convert this into an absorption coefficient per unit mass of Mb.

The absorption spectra normalized to sample areal density (defined as the mass of material per unit area) of four selected samples at hydration levels ranging from 3.6 to 42 wt % are shown in Figure 4. The error bars shown on each curve at several representative frequencies are standard deviations derived from multiple measurements for the same sample. The uncertainties increase at higher frequencies, as signal decreases with respect to the baseline noise level.

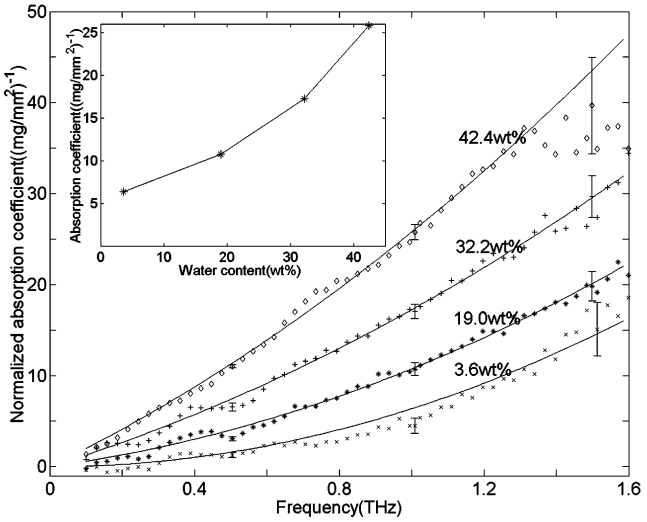

Figure 4. The absorption spectra of Mb samples from 3.6 to 42.2 wt % water content normalized to areal mass density, and the quadratic fit. Error bars at 0.5, 1.0, and 1.5THz are standard deviations derived from multiple measurements. The inset shows the absorption coefficient at 1.0 THz (the value on the fitting curves applied) for four samples. Weak oscillations at low frequencies are likely residual Fabry−Perot oscillations from the sample cell, and structures at high frequencies are noise due to weak signals and are within the error bars. These absorption spectra can be characterized as essentially smooth, continuous, and without sharp, identifiable features (see text).

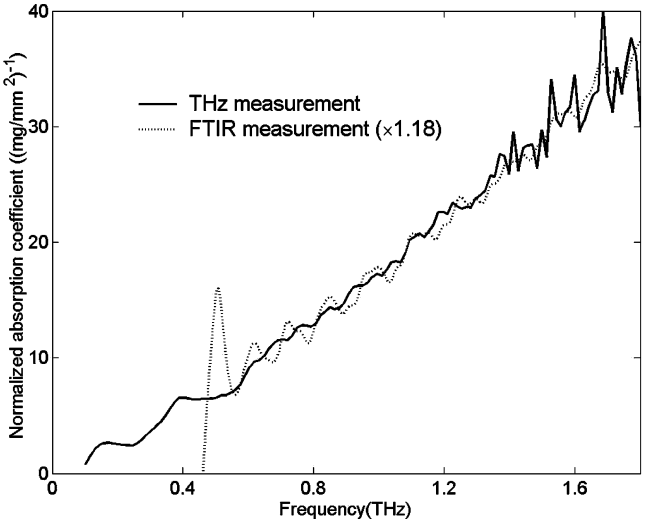

Figure 5. Comparison of absorption spectra obtained from THz and FTIR spectrometers for a Mb powder with 32.2 wt % water content. FTIR displays Fabry−Perot oscillations and increased uncertainty at low frequency due to weak source intensity, and requires normalization by a factor of 1.18 to coincide with the THz spectrum.

For all samples shown in Figure 4, the far-IR absorption spectra seen by THz-TDS show a fairly smooth increase with frequency. The spectra lack any identifiable absorption structures that can be assigned to the intrinsic vibrational or rotational modes of Mb. The weak oscillations seen at low frequencies likely are remnants of Fabry−Perot effects; the high-frequency peaks are smaller than the error bars and therefore not significant. Each absorption spectrum can be fit reasonably well by a simple quadratic curve, including spectra from many other specimens within this range of hydration levels. For the samples with higher hydration levels, e.g. 19.0, 32.2, and 42.2 wt %, it is clear that the water content is responsible for a major fraction of the THz absorption.

One might expect identifiable modes from large molecules at THz frequencies, but these data show smooth spectra. Recall that the THz absorption spectrum for water vapor consists of sharp lines, while liquid water has a continuous spectrum. A water molecule in the liquid phase experiences a wide range of instantaneous interaction potentials due to the highly variable arrangement of neighboring molecules, leading to an inhomogeneous broadening of the absorption spectrum. Hydrated Mb may have a highly variable arrangement of neighboring water molecules as well, leading to inhomogeneous broadening of the absorption spectrum, but this cannot account for the dehydrated Mb sample at 3.6 wt % water content.

Analysis of Mb absorption must be separated into two parts, the response of an ideal, single molecule of the protein, and the effect of an ensemble of many molecules with a wide range of individual conformations and configurations of neighboring molecules. For a single Mb molecule, calculations have been made for a particular set of effective potentials that find approximately 400 normal modes in the spectral region below 3 THz.[33] Since this leads to an average of two modes within 15 GHz spectrometer resolution, most modes would not be individually resolvable. These calculations do predict that the lowest lying modes below 0.5 THz will be separated by approximately 30 GHz, which should be resolvable by this spectrometer. The absence of such peaks in the measurements suggests that inhomogeneous broadening may be responsible. While Mb has a well-defined average structure, any real specimen will exhibit significant conformational disorder whereby the orientation of individual amino acid side chains and the number and location of biological waters varies from molecule to molecule. In addition, each protein molecule in the powder specimen can be in a slightly different local environment of neighboring protein molecules and biological waters, altering the local potential in a manner analogous to that in liquid water. The observed continuous absorption spectrum for even dehydrated Mb must arise from a combination of high mode density, conformational disorder, and variability in the local protein molecule environments.

Similar results are reported by Whitmire et al.[20] for THz-TDS studies of bacteriorhodopsin (BR) thin films. Although the calculated spectrum they obtained based on normal-mode analysis predicts some distinct absorption lines, their experimental results also show a broadly continuous nature.

IV.2. Comparison with FTIR Spectroscopy Measurements. To be certain that the continuous Mb absorption spectra are not artifacts of the THz spectrometer, selected samples were measured on a conventional FTIR spectrometer equipped with a composite silicon bolometer operating at 1.8 K[43] to extend the measurement range down to 1.0 THz. The same specimens and sample holders used in the THz-TDS measurements were used without modification for the FTIR measurements. For all samples, the absorption spectra obtained from two techniques are consistent within 20%. Results for powdered Mb with 32.2 wt % water content are showed in Figure 5. The systematic errors are potentially somewhat larger for FTIR in this very low-frequency range, but where comparable the FTIR spectra always show the same continuous spectra seen with THz-TDS. The good agreement with FTIR confirms the quantitative validity of THz-TDS, and that the continuous spectra are not artifacts of the THz spectrometer.

IV.3. Comparison with the Absorption Spectrum of Water Vapor. The far-IR absorption spectrum of water vapor is composed of distinct absorption lines due to vibrational and rotational motions of water molecules[27] and provides clear identification of water vapor in various environment.[12] While a

number of authors have investigated the potential of far-IR identification of specific biomolecules,[17,22,40,44−52] in which the size of the molecules is smaller than the sample we studied here, our results rule out this possibility for powdered Mb. Similar results can be expected for related proteins and other complex biomolecules.

V. Conclusions

The far-IR absorption spectra of powder Mb samples with water contents from 3.6 to 42 wt % were studied with THz-TDS and FTIR spectroscopy, and no identifiable absorption lines were found in any of the spectra. Absorption was dominated by the water content in all but the driest specimens. The continuous spectrum for a dehydrated specimen (3.6 wt %) shows that even dry Mb has broadened absorption properties, which is the apparent result of high normal mode density, conformational disorder, and configurational variability around individual Mb molecules. The use of THz-TDS for identification of large biomolecules through characteristic absorption features in the THz range does not appear to be possible, at least for biomolecules with complexities comparable to those of Mb. The use of single crystals and cryogenic temperatures may improve the observation of identifiable spectral features. THz-TDS is shown to be a sensitive probe of water in proteins, and should be useful for the study of biological water.

Acknowledgment. This work was supported by the Integrated Detection of Hazardous Materials (IDHM) Program, Purdue University, the Naval Surface Warfare Center, Crane, Indiana, and the National Science Foundation Award No. PHY-9988763.

References and Notes

(1) Auston, D. H.; Cheung, K. P.; Smith, P. R. *Appl. Phys. Lett.* **1984**, *45*, 284.
(2) Smith, P. R.; Auston, D. H.; Nuss, M. C. *IEEE J. Quantum Electron.* **1988**, *24*, 255.
(3) Vanexter, M.; Grischkowsky, D. R. *IEEE Trans. Microwave Theory Tech.* **1990**, *38*, 1684.
(4) Beard, M. C.; Turner, G. M.; Schmuttenmaer, C. A. *J. Phys. Chem. B* **2002**, *106*, 7146.
(5) Han, P. Y.; Tani, M.; Usami, M.; Kono, S.; Kersting, R.; Zhang, X. C. *J. Appl. Phys.* **2001**, *89*, 2357.
(6) Grischkowsky, D.; Keiding, S.; Vanexter, M.; Fattinger, C. *J. Opt. Soc. Am. B* **1990**, *7*, 2006.
(7) Krishnamurthy, S.; Reiten, M. T.; Harmon, S. A.; Cheville, R. A. *Appl. Phys. Lett.* **2001**, *79*, 875.
(8) Li, M.; Fortin, J.; Kim, J. Y.; Fox, G.; Chu, F.; Davenport, T.; Lu, T. M.; Zhang, X. C. *IEEE J. Sel. Top. Quantum Electron*. **2001**, *7*, 624.
(9) Kindt, J. T.; Schmuttenmaer, C. A. *J. Phys. Chem.* **1996**, *100*, 10373.
(10) Keiding, S. R. *J. Phys. Chem. A* **1997**, *101*, 5250.
(11) Knoesel, E.; Bonn, M.; Shan, J.; Heinz, T. F. *Phys. Rev. Lett.* **2001**, *86*, 340.
(12) Cheville, R. A.; Grischkowsky, D. *Opt. Lett.* **1995**, *20*, 1646.
(13) Jacobsen, R. H.; Mittleman, D. M.; Nuss, M. C. *Opt. Lett.* **1996**, *21*, 2011.
(14) Harde, H.; Zhao, J.; Wolff, M.; Cheville, R. A.; Grischkowsky, D. *J. Phys. Chem. A* **2001**, *105*, 6038.
(15) Nuss, M. C.; Mankiewich, P. M.; Omalley, M. L.; Westerwick, E. H.; Littlewood, P. B. *Phys. Rev. Lett.* **1991**, *66*, 3305.
(16) Kaindl, R. A.; Carnahan, M. A.; Orenstein, J.; Chemla, D. S.; Christen, H. M.; Zhai, H. Y.; Paranthaman, M.; Lowndes, D. H. *Phys. Rev. Lett.* **2002**, *88*, art. no. 027003.
(17) Markelz, A. G.; Roitberg, A.; Heilweil, E. J. *Chem. Phys. Lett.* **2000**, *320*, 42.
(18) Nagel, M.; Bolivar, P. H.; Brucherseifer, M.; Kurz, H.; Bosserhoff, A.; Buttner, R. *Appl. Phys. Lett.* **2002**, *80*, 154.
(19) Shen, Y. C.; Upadhya, P. C.; Linfield, E. H.; Davies, A. G. *Appl. Phys. Lett.* **2003**, *82*, 2350.
(20) Whitmire, S. E.; Wolpert, D.; Markelz, A. G.; Hillebrecht, J. R.; Galan, J.; Birge, R. R. *Biophys. J.* **2003**, *85*, 1269.
(21) Walther, M.; Fischer, B. M.; Jepsen, P. U. *Chem. Phys.* **2003**, *288*, 261.
(22) Johnston, M. B.; Herz, L. M.; Khan, A. L. T.; Kohler, A.; Davies, A. G.; Linfield, E. H. *Chem. Phys. Lett.* **2003**, *377*, 256.
(23) Eaves, J. D.; Fecko, C. J.; Stevens, A. L.; Peng, P.; Tokmakoff, A. *Chem. Phys. Lett.* **2003**, *376*, 20.
(24) Bahar, I.; Atilgan, A. R.; Demirel, M. C.; Erman, B. *Phys. Rev. Lett.* **1998**, *80*, 2733.
(25) Hill, J. R.; Tokmakoff, A.; Peterson, K. A.; Sauter, B.; Zimdars, D.; Dlott, D. D.; Fayer, M. D. *J. Phys. Chem.* **1994**, *98*, 11213.
(26) Hill, J. R.; Dlott, D. D.; Rella, C. W.; Peterson, K. A.; Decatur, S. M.; Boxer, S. G.; Fayer, M. D. *J. Phys. Chem.* **1996**, *100*, 12100.
(27) Vanexter, M.; Fattinger, C.; Grischkowsky, D. *Opt. Lett.* **1989**, *14*, 1128.
(28) Cheville, R. A.; Grischkowsky, D. *J. Opt. Soc. Am. B* **1999**, *16*, 317.
(29) Mittleman, D. M.; Nuss, M. C.; Colvin, V. L. *Chem. Phys. Lett.* **1997**, *275*, 332.
(30) Ronne, C.; Keiding, S. R. *J. Mol. Liq.* **2002**, *101*, 199.
(31) Kindt, J. T.; Schmuttenmaer, C. A. *J. Chem. Phys.* **1997**, *106*, 4389.
(32) Markelz, A.; Whitmire, S.; Hillebrecht, J.; Birge, R. *Phys. Med. Biol.* **2002**, *47*, 3797.
(33) Seno, Y.; Go, N. *J. Mol. Biol.* **1990**, *216*, 111.
(34) Melchers, B.; Knapp, E. W.; Parak, F.; Cordone, L.; Cupane, A.; Leone, M. *Biophys J.* **1996**, *70*, 2092.
(35) Dorbez-Sridi, R.; Cortes, R.; Mayer, E.; Pin, S. *J. Chem. Phys.* **2002**, *116*, 7269.
(36) Rudd, J. V.; Zimdars, D.; Warmuth, M. *Proc. SPIE* **2000**, *3934*, 27.
(37) Nuss, M. C.; Orenstein, J. Terahertz time-domain spectroscopy. In *Millimeter and Submillimeter Wave Spectroscopy of Solids*; Gruner, G., Ed.; Springer: New York, 1998.
(38) Han, H.; Park, H.; Cho, M.; Kim, J. *Appl. Phys. Lett.* **2002**, *80*, 2634.
(39) Duvillaret, L.; Garet, F.; Coutaz, J. L. *IEEE J. Sel. Top. Quantum Electron.* **1996**, 2, 739.
(40) Globus, T. R.; Woolard, D. L.; Khromova, T.; Crowe, T. W.; Bykhovskaia, M.; Gelmont, B. L.; Hesler, J.; Samuels, A. C. *J. Biol. Phys.* **2003**, *29*, 89.
(41) Duvillaret, L.; Garet, F.; Coutaz, J. L. *Appl. Opt.* **1999**, *38*, 409.
(42) Dorney, T. D.; Baraniuk, R. G.; Mittleman, D. M. *J. Opt. Soc. Am. A* **2001**, *18*, 1562.
(43) Infrared Laboratories Inc. 1808 E. 17th Street, Tucson, AZ 85719.
(44) Walther, M.; Fischer, B.; Schall, M.; Helm, H.; Jepsen, P. U. *Chem. Phys. Lett.* **2000**, *332*, 389.
(45) Kutteruf, M. R.; Brown, C. M.; Iwaki, L. K.; Campbell, M. B.; Korter, T. M.; Heilweil, E. J. *Chem. Phys. Lett.* **2003**, 375, 337.
(46) Walther, M.; Fischer, B. M.; Jepsen, P. U. *Chem. Phys.* **2003**, *288*, 261.
(47) Nagel, M.; Bolivar, P. H.; Brucherseifer, M.; Kurz, H.; Bosserhoff, A.; Buttner, R. *Appl. Opt.* **2002**, *41*, 2074.
(48) Mickan, S. P.; Menikh, A.; Liu, H. B.; Mannella, C. A.; MacColl, R.; Abbott, D.; Munch, J.; Zhang, X. C. *Phys. Med. Biol.* **2002**, 47, 3789.
(49) Fischer, B. M.; Walther, M.; Jepsen, P. U. *Phys. Med. Biol.* **2002**, 47, 3807.
(50) Walther, M.; Plochocka, P.; Fischer, B.; Helm, H.; Jepsen, P. U. *Biopolymers* **2002**, *67*, 310.
(51) Globus, T. R.; Woolard, D. L.; Samuels, A. C.; Gelmont, B. L.; Hesler, J.; Crowe, T. W.; Bykhovskaia, M. *J. Appl. Phys.* **2002**, *91*, 6105.
(52) Globus, T.; Bykhovskaia, M.; Woolard, D.; Gelmont, B. *J. Phys. D* **2003**, *36*, 1314.